Accepted version
Licence CC BY 4.0
Please cite as:

Larsen, H.C., Mohn, G., Nirrengarten, M. *et al.* Rapid transition from continental breakup to igneous oceanic crust in the South China Sea. *Nature Geosci* **11,** 782–789 (2018). https://doi.org/10.1038/s41561-018-0198-1

Rapid transition from continental breakup to oceanic crust at South China Sea rifted margin

H. C. Larsen[a*], G. Mohn[b*], M. Nirrengarten[b], Z. Sun[c], J. Stock[d], Z. Jian[e], A. Klaus[f], C. Alvarez-Zarikian[f], J. Boaga[g], S. A. Bowden[h], A. Briais[i], Y. Chen[j], D. Cukur[k], K. Dadd[l], W. Ding[m], M. Dorais[n], E. Ferre[o], F. Ferreira[p], A. Furusawa[q], A. Gewecke[r], J. Hinojosa[d], T. W. Höfig[f], K. Hsiung[s], B. Huang[t], E. Huang[e], X. Huang[u], S. Jiang[v], H. Jin[t], B. Johnson[w], R. Kurzawski[x], C. Lei[y], B. Li[z], L. Li[e], Y. Li[aa], J. Lin[ab], C. Liu[ac], C. Liu[e], Z. Liu[e], A. Luna[ad], C. Lupi[ae], A. McCarthy[af], L. Ningthoujam[ag], , N. Osono[ah], D. W. Peate[ai], P. Persaud[ac], N. Qiu[c], C. Robinson[aj], S. Satolli[ak], I. Sauermilch[al], J. C. Schindlbeck[x], S. Skinner[am], S. Straub[an], X. Su[c], C. Su[ao], L. Tian[ap], F. M. van der Zwan[aq], S. Wan[ar], H. Wu[as], R. Xiang[c], R. Yadav[ag], L. Yi[e], P., C. Zhang[c], J. Zhang[c], Y. Zhang[at], N. Zhao[ab], G. Zhong[e], L. Zhong[au]

[a] School of Ocean and Earth Science, Tongji University, 1239 Siping Road, Shanghai 200092, China
[b] Laboratoire Géosciences et Environnement Cergy (GEC), Maison Internationale de la Recherche, Université de Cergy-Pontoise, 1, rue Descartes, 95000 Neuville-sur-Oise, France

*Corresponding Authors. hclarseniodp@gmail.com, geoffroy.mohn@u-cergy.fr

The style of magmatism at rifted margins differs widely from margins with transient, abundant magmatism (magma-rich), to magma-poor margins. The latter type is characterized by extreme continental lithospheric thinning resulting in ~100 km-wide zones of mantle exhumation, and a delayed initiation of igneous oceanic crust formation. This discovery caused a change in rifted margin paradigms, raised fundamental questions on the onset of ocean-floor type magmatism, and has guided interpretation of seismic data across many other rifted margins, including the highly extended northern South China Sea (SCS) margin. International Ocean Discovery Program (IODP) expeditions 367/368 to the northern SCS tested the magma-poor margin model outside North Atlantic for the first time. Contrary to model predictions, results show initiation of MORB-type (Mid-Ocean Ridge) basaltic magmatism during final breakup, and a narrow, rapid transition into igneous oceanic crust formation. Cores suggest that crustal extension was fast, and do not show evidence for mantle exhumation. Rapid crustal thinning within a relatively thin pre-rift lithosphere may have caused asthenosphere upwelling that yielded early MORB-type magmatism from normal temperature mantle during continental breakup.

Continental breakup represents the successful process of rifting, weakening and thinning of the continental lithosphere eventually leading to complete plate rupture ('final breakup'). IODP expeditions 367/368 at the northern South China Sea (SCS) margin (Fig. 1) offer an opportunity to explore the spectrum of breakup processes defined by the two end-members identified by North Atlantic drilling[1,2]: magma-rich and magma-poor margins[3]. The SCS margin shows none of the expected characteristics of magma-rich margins[4,5] such as transient formation of excessively thick igneous crust (15-30 km) and >5 km thick seaward-dipping reflectors (e.g. East Greenland margin[6,7]). Instead, its structural architecture, as inferred from seismic data, is reminiscent of a hyperextended, ´magma-poor margin[8–11]. Our findings reveal the first well-constrained example of the 'missing link' between magma-rich margins and magma-poor, hyperextended margins. Formation of such intermediate type margins has previously been reported (e.g. Gulf of California[12], Red Sea[13]), but not confirmed by drilling.

Figure 1: A. Topographic map of the SCS[14] with the location of IODP/ODP Sites[15–17]. Sedimentary basins: Pearl River Mouth Basin (PRMB), Liwan Basin (LB), Ocean Sub-basins: Eastern Sub-Basin (ESB), North West Sub-Basin (NWSB), South West Sub-Basin (SWSB);

Continental domains: IC: Indochina, PW: Palawan, P: Philippines, TW: Taiwan. B. Depth to acoustic basement (Tg) presented with the seismic lines[18] used in Figure 2 and indication of distinct topographic features: Outer Margin High (OMH) and Ridges A, B and C. Note the presence of a transform fault west of the margin segment we investigate. For both maps, picking of magnetic anomalies are after [19,20] with geomagnetic time scale of [21]. Gridded magnetic data can be found in [19,22].

Tectonic setting of the SCS oceanic basin

The SCS oceanic basin formed during the early Oligocene to middle Miocene (32-15 Ma)[16,23]. Its development includes the formation of several sub-basins (Fig. 1A) and rift propagation events. Our study focuses on a ~100 km-long segment[18] at the northern SCS margin within the north-west oceanic sub-basin (Fig. 1B). Previous studies suggest major rifting during late Eocene time and final breakup during the early Oligocene[16,24]. Earlier extension events have been suggested based on pre-late Eocene, non-marine sediments within the deep part of the Pearl River Mouth Basin[24,25] located on the inner part of the ~400 km wide SCS margin (Fig. 1A). However, evidence for major pre-late Eocene rifting in the distal margin of the SCS is neither supported by seismic data (Figs. 1B and 2a) that show only a single, strong rifting event, nor recovered by drilling. Our drilling study covers this distal ~ 200 km wide margin where continental breakup took place, and extends seawards from the deep Liwan Basin to oceanic crust (Figs. 1B and 2a). This specific margin segment has been interpreted as magma-poor, possibly hosting exhumed lower crust and upper mantle in its distal parts[18,26]. The conjugate Palawan margin (Fig. 1) is much less constrained, but a late Eocene to early Oligocene rifting across a 150-200 km zone is reported[27]. Widespread, possibly plume-related post-spreading magmatism across the margin[28,29], however remains conjectural in light of our findings.

General structure of the northern SCS margin

The Liwan Basin is characterized by highly thinned crust, ≤10 km below the deepest rift basins (Fig.2a), that formed in response to extensive normal faulting[4,24]. One major rifting event can be identified from the seismic data, ending somewhere between unconformity T80 (~30 Ma) and T60 (~26 Ma; Fig. 2a). Most extensional faults sole out within a major decollement zone at mid- to top of lower-crustal level (Fig. 2a). The Liwan Basin is bounded to the SE by the Outer Margin High (OMH). The major decollement zone is interpreted to continue laterally below the OMH, but cannot be followed with confidence seaward of the OMH (Fig. 2a). The lower crust is thinnest (~8 km) beneath the deep rift basins, but thickens below, and possibly seawards of the OMH, suggesting that the lower crust remained ductile and able to flow during rifting as also observed by previous studies[30,31]. Lower crustal flow may have continued beyond final breakup and caused local post-rift margin deformation[32].

Three distinct parallel basement ridges (A, B and C) trending west-southwest to east-northeast are present at the most distal margin (Figs. 1B, 2a, b, c and supplementary material) between 115°40'E and 116°40'E. Ridge A shows significant morphological variation (depth, width, reflection character) along strike, and sub acoustic basement (Tg) reflectors cannot be regionally interpreted with any confidence (Fig. 2a, b, c, e). However, the continental Moho can be followed to and below Ridge A where the crust is only 2 – 2.5 s (TWT; ~7-9 km) thick (Fig. 2a, b, c).

Ridges B and C are well defined by seawards-dipping bounding faults offsetting Tg, and show remarkable lateral continuity and smooth basement surfaces (Figs. 1B, 2a, b, c, f, g and supplementary material). Magnetic anomaly C11n (~29.5 Ma; Fig. 1)[19,33] is located close to Ridge B. Ridge C is within anomaly C10r (~28.8 – 29.4 Ma) and C10n (~28.7 Ma) is placed seaward of it (Figs. 1B and 2 a, b ,c), implying initial seafloor half-spreading rate of ~2.5 cm/yr[19,33].

In contrast to the continental Moho reflector below Ridge A, the Moho reflector beneath Ridges B and C is more patchy, although its depth is consistent with regional wide-angle seismic data[34] that show ~6 km-thick crystalline crust with $V_p > 5$ km/s from this location and seawards into younger oceanic crust. Crustal seismology and magnetic anomalies therefore suggest that the transition from continental crust to full oceanic crust is located between Ridge A and Ridge C.

Drilling results and correlation to seismic data

IODP Site U1501 on the crest of the OMH (Figs. 2a, d) recovered two lithostratigraphic units above the acoustic basement reflector Tg[35]. These two units are separated by unconformity T60 (~26 Ma) and they span the entire syn- and post-rift basin development: Unit 1 of early

Miocene to Pleistocene age contains deep marine calcareous-rich sediment and ooze; and Unit 2 comprising late Eocene to late Oligocene siliciclastic sediments (Fig. 3)[35]. The base of the ~300-m-thick Unit 2 contains coarse sand intervals (shallow marine) with up to pebble-sized clasts, interbedded with mm thin beds of lignite or coal and glauconite-bearing sand. Up-section, it shows overall fining of clastic material reflecting deepening basin conditions from (base) shallow marine to (top) bathyal depths. The sedimentary facies of the deeper part of Unit 2 is similar to the late Eocene Enping Formation recovered from industry boreholes within the Pearl River Mouth Basin[36], and is interpreted as reflecting the main SCS rifting event[24]. Site U1435[37] near the continent-ocean transition (Fig. 1) recovered similar types of syn-rift sediments. It is noteworthy, however, that neither seismic data, nor coring data shows the presence of a distinct breakup unconformity within Unit 2 encompassing the entire syn-rift to early post-rift development. In particular, the T80 reflector (~30 Ma) is only represented in the cores by an upwards increase in calcareous nanno-fossils within the siliciclastic clay dominating T83-T80 interval. A marked change in the ratio between pelagic and benthic foraminifers upwards from T80 suggests basin deepening from shelf slope to bathyal depths[35] following final breakup within the most distal margin.

Figure 2: Interpreted seismic sections (see location in Figure 1). Drill sites marked with 'p' are projected. a. regional seismic profile crossing the northern SCS margin. b and c. expanded views of Ridges A, B, C emphasizing their lateral continuity. d, e, f display seismic sections across the drilling sites. g. is a line drawing from a strike line across Ridge B showing a mound-like structure below Site U1500 suggesting that slightly younger volcanic strata may sub-crop elsewhere along the ridge. Seismic data courtesy of Chinese National Offshore Oil and Gas Company (CNOOC). CNOOC convention for naming seismic stratigraphic unconformities[38,39] has been adapted. Regional seismic stratigraphic unconformities T30-T83

with ages obtained from IODP drill cores. T60 unconformity reflects some late, post rift deformation of minimal extension, possibly related to lower crustal flow[32]. Tg: Acoustic basement is not representing a time line or specific stratigraphic relationships of lithologies (see Figure 3). Black line: Moho reflector (verified directly below Ridge B by wide angle data[34]).

The material recovered from below the highly reflective Tg reflector is a strongly lithified sandstone to conglomerate displaying a sharp, major increase in density and P-wave velocities, and a sudden decrease in porosity (~20% to ~5%)[35]. An angular unconformity at Tg of about 15° is observed in the cores, and seismic data show a nearby, strong erosional truncation of a syncline (Fig. 2d and supplementary material). Together, this implies that Tg represents a major hiatus between sediments suffering pre-rift deformation and compaction (Cretaceous?), and deposition of the overlying syn-rift deposits (Unit 2).

Figure 3: Summary chart of drilling results. Ages based on core samples analyzed for calcareous nannofossils, foraminifers, diatoms, and ostracods; lithostratigraphy from detailed core descriptions[35,40–42] following the GTS12[43] geological timescale.

IODP Sites U1499 and U1502 sampled Ridge A (Figs. 2a, b, c, e), but yielded widely different results. The lower intervals of Site U1499[40] (Fig. 3) consist, from top to bottom, of: 1) post-rift, lower Miocene fine-grained red claystone, 2) coarse siliciclastic sediments composed of a sandy matrix-supported breccia with angular pebble-sized sedimentary clasts bearing ages spanning from early Miocene (~23 Ma) through early Oligocene (~30 Ma)[40], 3) undated, moderately lithified gravel composed mostly of polygenic cobble-sized clasts. The clasts predominantly consist of previously eroded sedimentary rocks (mostly coarse-grained sandstone).

Site U1502 is located 40 km east of Site U1499 along Ridge A (Figs. 1, 2e). In the seismic profiles (Fig. 2e), a highly reflective Tg is dipping ~25°, and is overlain by moderately dipping to sub-horizontal on-lapping sedimentary layers of mainly post-rift age. Below Tg, a total of 180 m of basaltic lavas with pillow structures were recovered, and are immediately overlain (Fig. 3) by a condensed sequence of fine grained, deep-marine sediments ranging in age from early Oligocene (~30 Ma) to early Miocene (~23 Ma)[42]. Clay to claystone immediately above the basalts document an assemblage of agglutinated benthic foraminifers that, if indeed in-situ material, could indicate a late Eocene age[42]. The entire basalt sequence suffered pervasive hydrothermal alteration reaching greenschist facies conditions and profound brecciation (hydro-fracturing) associated with abundant iron-sulphide mineralization[42]. This hydrothermal activity extends into the lowermost part (~5m) of the overlying, deep-marine sediments of early Oligocene age (Fig. 3), implying that no major hiatus exists between igneous activity and sedimentation. This effectively constrains the basaltic activity to 30-34 Ma during the final stages of continental breakup. Their strong and seaward rotation differs from that of Ridge B (~5° landward rotation), and is consistent with late stage deformation at the most distal continental margin prior to onset of margin-wide magmatism at Ridge B.

The continuation of the continental Moho (Fig. 2a, b, c) below Ridge A implies that this ridge is floored by continental crust. There is no indication of magmatism at Site U1499 at the time of continental breakup. Instead, matrix-supported breccia and gravels were recovered at Site U1499 below Tg, and possibly were deposited by syn-tectonic gravity flows in response to rifting. The gravels have a large proportion of upper crustal materials, in part sedimentary origin, suggesting limited, if any, deep tectonic exhumation in the source area. Overall, this suggests that Ridge A records the interplay between late-stage continental extension and breakup related magmatism.

Site U1500 on the landwards tilted (~5°) fault block of Ridge B (Fig. 2f, g) recovered 1380 m of deep marine Neogene to Oligocene sediments overlying 150 m of volcanic basement[41]. The fresh to moderately altered basaltic lavas alternate between thick massive flows and pillow flows (Fig. 3). Very thin intercalated sediment layers are present within the lavas. Nannofossils of Oligocene age within these sediments are consistent with the presence of upper Oligocene to lower Miocene post-basaltic sediments, and with the alignment of magnetic chron C11n (29.5 Ma) with Ridge B (Figs. 1, 2a, b, c and 3).
The along-ridge seismic line shows that the basement sampled at Site U1500 is acoustically layered down to ~2 km below Tg (Vp of 4.5 – 5.0 km/s) in a similar fashion as the cored upper 150 m, and this extends all along Ridge B (Fig. 2f, g and supplementary material). This suggests that a ~2 km (minimum) thick volcanic edifice is present at this ridge. While this implies considerable basaltic magmatism along the entire Ridge B around Chron C11n time, it does not unambiguously prove that full oceanic crust is present below Ridge B. A thick extrusive cover might be sufficient to generate the magnetic anomaly, even if it is floored by remnants of continental lithosphere. Ridge B, however, shares the characteristic features of Ridge C (as opposed to the continental Ridge A), which, except for its fault-bounded nature, forms a straight continuation into the younger SCS oceanic crust.

Importantly, the composition of the basalts from ridges A and B forms a continuum with that of the igneous oceanic crust sampled by IODP Expedition 349 within the younger SCS basin[16]. Sites U1500 and U1502 lavas all have MORB compositions (Fig. 4) with MORB-like petrography: plagioclase phyric, olivine-bearing, lacking clinopyroxene phenocrysts. This is consistent with mantle-derived primitive, dry melts, generated by decompression melting in a mid-ocean-ridge setting. From this, we conclude that a melting regime comparable to a mature spreading centre in terms of melt composition, productivity and lateral extent was present during the time of final rifting and breakup (Ridge A to Ridge B stage) and continued to operate during the subsequent SCS formation (Ridge C and younger).

The normal faults of Ridges B and C show significant displacements (up to ~500 m) of Tg representing igneous basement and the very oldest post-breakup sediments, but do not offset the younger sediments of latest Oligocene to early Miocene sediments. This fault activity therefore occurred within a short time interval (mid-Oligocene) during or just after the formation of the igneous basement and is, in this regard, reminiscent of abyssal hill type topography. The modest (~5°) block rotation, however, suggests that only minor tectonic extension operated in tandem with the igneous crustal accretion during final breakup to early seafloor spreading.

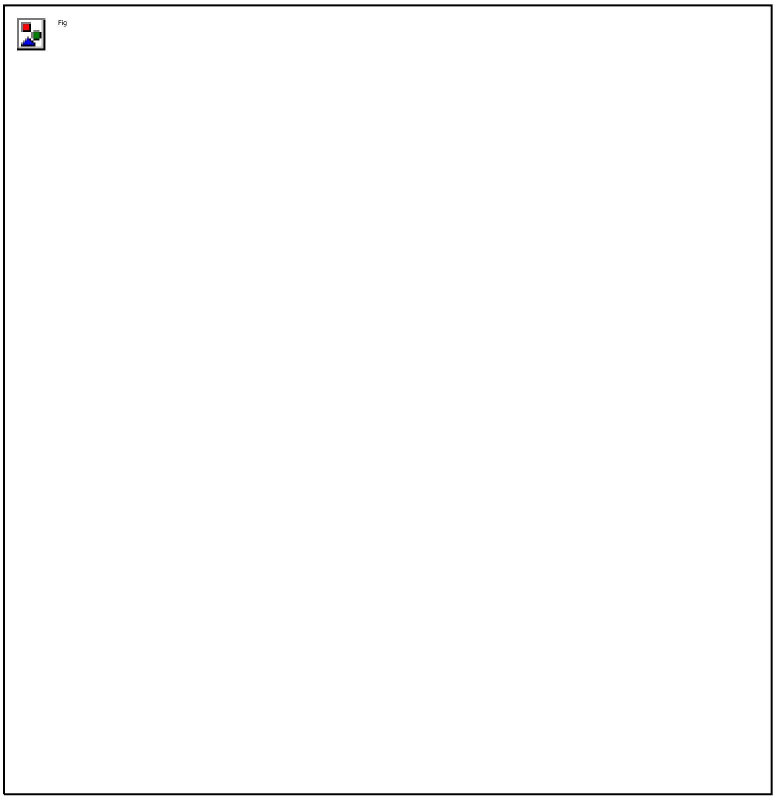

Figure 4: Ti-V discrimination diagram[44] of basalts sampled by IODP expeditions 367-368 on the rifted margin (Sites U1500 and U1502)[41,42] and IODP 349 sites located on oceanic crust[16]. (See supplementary material 3)

Discussion and conclusion

A single and major rifting event of late Eocene to early Oligocene age (~37-30 Ma) on the outer, distal margin of the northern SCS is inferred by both seismic observations and drilling results. The drilling data support a kinematic history of the SCS with breakup at around magnetic chron C11n (~30 Ma), but the finding of extensive MORB-type magmatism at final breakup time contradicts prior studies suggesting a magma-poor margin involving mantle exhumation and magma starvation[26]. Similarly, cores show no evidence for late-stage, post breakup magmatism hypothesized to overprint the margin[28].

Combined with seismic data, drilling results strongly suggest that Ridge A is floored by continental crust, but locally experienced MORB magmatism within its eastern part (i.e. Site U1502), potentially reflecting an east to west propagation of initial margin magmatism. The age of this magmatism is constrained to between 30 Ma and 34 Ma. Ridge B, on the contrary, has a ridge-long cover of at least 2 km thick volcanics (MORB-type) of early Oligocene age (Fig. 2g and Fig. 3), aligns with magnetic Chron C11n anomaly (~30 Ma), and is in most aspects comparable to Ridge C. However, it cannot be excluded that Ridge B represents transitional crust (Fig. 5), as opposed to mature oceanic igneous crust that subsequently formed. This uncertainty in the location of the rift-to-drift transition is only ~20 km (Stages 2-3 in Fig. 5) and equivalent to ~1 Myr in time (assuming an average half-extension rate of 2 cm/yr or higher between ridges A and C).

A key characteristic of the northern SCS margin revealed by the IODP cores, therefore is a short (~7 Myrs) rifting event with a narrow, and by implication, rapid rift-to-igneous crustal accretion transition, which is in marked contrast with the magma-poor Iberia-Newfoundland margins recording more than ~30 Myrs of crustal rifting and subcontinental mantle exhumation prior to igneous crustal accretion[11,45].

Figure 5: Conceptual model of continental breakup based on integration of seismic and drilling data (Figs. 2, 3). Stage 1: a deep basin with thin crust existed within final zone of plate rupture and hosted magmatism between 34 – 30 Ma. Stage 2: Ascending melts rapidly weakened the mantle lithosphere and massive extrusive activity along the entire rift zone takes place, underpinned by a thicker zone of melting in the asthenosphere. Stage 3: Seafloor spreading and passive upwelling of asthenospheric mantle is established. Igneous basement of Ridges B and C are affected by normal faults. Note that in time, stages 2 and 3 are ~ 1 Myr apart (or less), but a high rate (~ 2.5 cm/yr, half-rate) of plate separation translates to significant distance in space. The area of possible transient crust around Ridge

B is shown in purple. Constraints on the southern conjugate margin (Palawan) structure are limited to seismic data of moderate quality[27] and only schematically represented. However, both the timing of rifting at the distal margin and the width of the zone of main crustal necking are similar on both margins.

Establishment of a mantle-melting regime yielding MORB-type magmatism at, or even slightly before (i.e., Site U1502), final breakup is readily explained at magma-rich margins by emplacement of anomalously hot asthenosphere[6,46]. However, the lack of the distinct characteristics of magma-rich margins at the SCS implies the need for a different model for this margin. Instead, we suggest that rifting of the SCS margin, involving a major and fast episode of extension during late Eocene to early Oligocene time enabled formation of sufficient decompression melting within the asthenosphere to initiate the passive asthenospheric upwelling eventually needed to form full igneous crust from normal temperature mantle (Fig. 5). Assuming an original crustal thickness of ~30 km, the only ~8 km thick residual continental crust below Ridge A implies a stretching factor of ~4. Normal temperature asthenospheric mantle can in this case lead to significant melt production[47,48]. For Ridge B, where residual continental crust is ~4 km or less, melt supply could be very high and approach that of full oceanic crust. However, in addition to the amount of stretching, rift duration also has profound impact on melt yields[49]. High extension rates imply fast vertical ascent of asthenospheric mantle that suppresses heat loss through conduction and, provided focused upwelling takes place, normal thickness oceanic crust can form[48,49]. The relatively high rate of spreading recorded in the SCS after breakup (2.5 cm/yr, half rate) exceeds the threshold of ~1 cm/yr ascent rate considered a limit for effective supply of crust forming melts during steady state spreading[50].

If we further consider that the SCS margin formed within relatively young and hot lithosphere[30,31] with a thickness (present day) of only 80 km[51], melt generation would initiate at lower stretching factors compared to normal conditions[49]. Ascent of early melts (Fig. 5) provides for convective heat transfer into the lithosphere[52,53], can favor grain boundary sliding leading to reduced viscosity[54], and effectively aids extension and rift localization during late stage rifting[13]. The decoupling of extension between crust and mantle by a ductile lower crust may have contributed to this process by allowing the mantle lithosphere to extend independently of the crust in both time and space[13,30,55]. The presence of a relatively thin pre-breakup lithosphere that dominantly deformed in a pure shear mode is independently supported by modeling of the anomalously high heat-flow (~100 mW/m^2 Site 1499 and 1501[35,40]) characterizing the margin[56] and by the observation of lower crustal flow[32].

In summary, our drilling results suggest that rapid rifting in a relative thin, young lithosphere was conducive for establishing a mantle flow pattern that yielded ocean floor type (MORB-type) melts (amount and composition) during final breakup and early seafloor spreading, and resulted a narrow and fast rift-to-drift transition along a ~100 km long segment of the northern SCS margin.

Acknowledgement: We are indebted the Chinese National Offshore Oil and Gas Company (CNOOC) to provide access for Z.S. and H.C.L. to work on their large regional database of seismic reflection data, which CNOOC subsequently amended with acquisition of new data to document our selected drill sites. We are thankful to the Joides Resolution crew and the IODP technical staff. IODP-China office supported international workshops to develop the original drilling proposal. Co-PI's of the drilling proposal Pinxian Wang and Chun-Feng Li are acknowledged for their contributions to planning. The Editor, Tim Minshull and an anonymous reviewer provided most helpful comments. This research used data and samples provided by the International Ocean Discovery Program. A.K. and C.A-Z. acknowledge support by NSF award OCE-1326927.

References:

1. Doré, T. & Lundin, E. Hyperextended continental margins — Knowns and unknowns. *Geol.* **43,** 95–96 (2015).
2. Peron-Pinvidic, G., Manatschal, G. & Osmundsen, P. T. Structural comparison of archetypal Atlantic rifted margins: A review of observations and concepts. *Mar. Pet. Geol.* **43,** 21–47 (2013).
3. Franke, D. Rifting, lithosphere breakup and volcanism: Comparison of magma-poor

and volcanic rifted margins. *Mar. Pet. Geol.* **43,** 63–87 (2013).

4. Gao, J. *et al.* The continent–ocean transition at the mid-northern margin of the South China Sea. *Tectonophysics* **654,** 1–19 (2015).
5. Lester, R. *et al.* Rifting and magmatism in the northeastern South China Sea from wide-angle tomography and seismic reflection imaging. *J. Geophys. Res. Solid Earth* **119,** 2305–2323 (2014).
6. Holbrook, W. S. *et al.* Mantle thermal structure and active upwelling during continental breakup in the North Atlantic. *Earth Planet. Sci. Lett.* **190,** 251–266 (2001).
7. Larsen, H. C. & Saunders, A. D. in *Proceedings of the Ocean Drilling Program, 152 Scientific Results.* **152,** (Ocean Drilling Program, 1998). doi:10.2973/odp.proc.sr.152.240.1998
8. Boillot, G., Winterer, E. L. & Al., E. in *Proceedings of the Ocean Drilling Program, 103 Scientific Results*. **103,** (Ocean Drilling Program, 1988).
9. Minshull, T. A. Geophysical characterisation of the ocean–continent transition at magma-poor rifted margins. *Comptes Rendus Geosci.* **341,** 382–393 (2009).
10. Tucholke, B. & Sibuet, J.-C. *Proceedings of the Ocean Drilling Program, 210 Scientific Results*. **210,** (Ocean Drilling Program, 2006).
11. Whitmarsh, R. B., Manatschal, G. & Minshull, T. A. Evolution of magma-poor continental margins from rifting to seafloor spreading. *Nature* **413,** 150–4 (2001).
12. Lizarralde, D. *et al.* Variation in styles of rifting in the Gulf of California. *Nature* **448,** 466–9 (2007).
13. Ligi, M. *et al.* Birth of an ocean in the Red Sea: Initial pangs. *Geochemistry, Geophys. Geosystems* **13,** (2012).
14. Amante, C. & Eakins, B. W. ETOPO1 1 Arc-Minute Global Relief Model: Procedures, Data Sources and Analysis. *NOAA Tech. Memo. NESDIS NGDC-24. Natl. Geophys. Data Center, NOAA* (2009). doi:10.7289/V5C8276M
15. Wang, P., Prell, W. L. & Blum, P. *Proceedings of the Ocean Drilling Program, 184 Initial Reports*. **184,** (Ocean Drilling Program, 2000).
16. Li, C.-F., Lin, J., Kulhanek, D.K., & Expedition 349 Scientists. *Proceedings of the International Ocean Discovery Program, 349: South China Sea Tectonics*. **349,** (International Ocean Discovery Program 2015). doi:10.14379/iodp.proc.349.102.2015.

17. Sun, Z., Jian, Z. Stock, J.M., Larsen, H.C., Klaus, A., Alvarez Zarikian, C.A., & Expedition 367/368 Scientists. *Proceedings of the International Ocean Discovery Program Volume **367/368***. (International Ocean Discovery Program 2018). doi:10.14379/iodp.proc.367368.2018

18. Sun, Z., Stock, J., Jian, Z., Larsen, H.-C., Alvarez Zarikian, C.A., and Klaus, A. *Expedition 367/368 Scientific Prospectus Addendum: South China Sea Rifted Margin*. (International Ocean Discovery Program, 2016). doi:10.14379/iodp.sp.367368add.2016

19. Briais, A., Patriat, P. & Tapponnier, P. Updated interpretation of magnetic anomalies and seafloor spreading stages in the south China Sea: Implications for the Tertiary tectonics of Southeast Asia. *J. Geophys. Res.* **98,** 6299 (1993).

20. Seton, M. *et al.* Community infrastructure and repository for marine magnetic identifications. *Geochemistry, Geophys. Geosystems* **15,** 1629–1641 (2014).

21. Gee, J. S. & Kent, D. V. Source of Oceanic Magnetic Anomalies and the Geomagnetic Polarity Timescale. *Treatise Geophys.* **5,** 455–507 (2007).

22. Ishihara, T., Kisimoto, K. Magnetic anomaly map of East Asia 1:4.000.000, [CD- ROM]. (1996).

23. Taylor, B. & Hayes, D. Origin and history of the South China Sea basin. *Tecton. Geol. Evol.* **27,** (1983).

24. Zhou, D., Ru, K. & Chen, H. Kinematics of Cenozoic extension on the South China Sea continental margin and its implications for the tectonic evolution of the region. *Tectonophysics* **251,** 161–177 (1995).

25. Ru, K. & Pigott, J. D. Episodic rifting and subsidence in the South China Sea. *Am. Assoc. Pet. Geol. Bull.* **70,** 1136–1155 (1986).

26. Franke *et al.* The final rifting evolution in the South China Sea. *Mar. Pet. Geol.* **58,** 704–720 (2014).

27. Franke, D. *et al.* The continent-ocean transition at the southeastern margin of the South China Sea. *Mar. Pet. Geol.* **28,** 1187–1204 (2011).

28. Fan, C. *et al.* New insights into the magmatism in the northern margin of the South China Sea: Spatial features and volume of intraplate seamounts. *Geochemistry, Geophys. Geosystems* **18,** 2216–2239 (2017).

29. Zhao, F. *et al.* Prolonged post-rift magmatism on highly extended crust of divergent

continental margins (Baiyun Sag, South China Sea). *Earth Planet. Sci. Lett.* **445,** 79–91 (2016).

30. Brune, S., Heine, C., Clift, P. D. & Pérez-Gussinyé, M. Rifted margin architecture and crustal rheology: Reviewing Iberia-Newfoundland, Central South Atlantic, and South China Sea. *Mar. Pet. Geol.* **79,** 257–281 (2017).
31. Clift, P., Lin, J. & Barckhausen, U. Evidence of low flexural rigidity and low viscosity lower continental crust during continental break-up in the South China Sea. *Mar. Pet. Geol.* **19,** 951–970 (2002).
32. Clift, P. D., Brune, S. & Quinteros, J. Climate changes control offshore crustal structure at South China Sea continental margin. *Earth Planet. Sci. Lett.* **420,** 66–72 (2015).
33. Li, C.-F. *et al.* Ages and magnetic structures of the South China Sea constrained by deep tow magnetic surveys and IODP Expedition 349. *Geochemistry, Geophys. Geosystems* **15,** 4958–4983 (2014).
34. Pin, Y., Di, Z. & Zhaoshu, L. A crustal structure pro file across the northern continental margin of the South China Sea. *Tectonophysics* **338,** (2001).
35. Larsen, H.C., Jian, Z., Alvarez Zarikian, C.A., Sun, Z., Stock, J.M., Klaus A. &Expedition 367/368 Scientists. Site U1501 in *Proceedings of the International Ocean Discovery Program Volume 367/368*. (International Ocean Discovery Program 2018) doi:10.14379/iodp.proc.367368.105.2018
36. Pinglu, L. & Chuntao, R. Tectonic characteristics and evolution history of the Pearl river mouth basin. *Tectonophysics* **235,** 13–25 (1994).
37. Li, C.-F., Lin, J., Kulhanek, D.K., & Expedition 349 Scientists. Site U1435 in *Proceedings of the International Ocean Discovery Program, 349: South China Sea Tectonics*, (International Ocean Discovery Program 2015) doi:10.14379/iodp.proc.349.107.2015.
38. Dai, Y., Yu, Q., Li, H., Wang, Z., Bai, J., and Peng, H. Threshold conditions and reservoir-controlling characteristics of source kitchen in Zhu I depression, Pearl River Mouth Basin. *Acta Pet. Sin.* **36,** 145–155 (2015).
39. Shi, H., He, M., and Zhang, L. Hydrocarbon geology, accumulation pattern and the next exploration strategy in the eastern Pearl River Mouth basin. *China Offshore Oil Gas* **26,** 11–22 (2014).
40. Sun, Z., Stock, J.M., Klaus, A., Larsen, H.C., Jian, Z., Alvarez Zarikian C.A. & Expedition 367/368 Scientists. Site U1499 in *Proceedings of the International Ocean Discovery*

Program Volume 367/368. (International Ocean Discovery Program 2018). doi:10.14379/iodp.proc.367368.103.2018.

41. Stock, J.M., Sun, Z., Klaus, A., Larsen, H.C., Jian, Z., Alvarez Zarikian C. & Expedition 367/368 Scientists. Site U1500 in *Proceedings of the International Ocean Discovery Program Volume 367/368*. (International Ocean Discovery Program 2018). doi:10.14379/iodp.proc.367368.104.2018.
42. Larsen, H.C., Jian, Z., Alvarez Zarikian, C.A., Sun, Z., Stock, J.M., Klaus A. & Expedition 367/368 Scientists. Site U1502 in *Proceedings of the International Ocean Discovery Program Volume 367/368*. (International Ocean Discovery Program 2018). doi:10.14379/iodp.proc.367368.106.2018.
43. Gradstein, F. M. & Ogg, J. G. in The Geologic Time Scale 31–42 (Elsevier, 2012). doi:10.1016/B978-0-444-59425-9.00002-0.
44. Shervais, J. W. Ti-V plots and the petrogenesis of modern and ophiolitic lavas. *Earth Planet. Sci. Lett.* **59,** 101–118 (1982).
45. Minshull, T. A., Dean, S. M., White, R. S. & Whitmarsh, R. B. Anomalous melt production after continental break-up in the southern Iberia Abyssal Plain. *Geol. Soc. London, Spec. Publ.* **187,** 537–550 (2001).
46. White, R. & McKenzie, D. Magmatism at rift zones: The generation of volcanic continental margins and flood basalts. *J. Geophys. Res.* **94,** 7685 (1989).
47. Fletcher, R., Kusznir, N. & Cheadle, M. Melt initiation and mantle exhumation at the Iberian rifted margin: Comparison of pure-shear and upwelling-divergent flow models of continental breakup. *Comptes Rendus - Geosci.* **341,** 394–405 (2009).
48. Mckenzie, D. & Bickle, M. J. The volume and composition of melt generated by extension of the lithosphere. *J. Petrol.* **29,** 625–679 (1988).
49. Bown, J. W. & White, R. S. Effect of finite extension rate on melt generation at rifted continental margins. *J. Geophys. Res. Solid Earth* **100,** 18011–18029 (1995).
50. Lizarralde, D., Gaherty, J. B., Collins, J. A., Hirth, G. & Kim, S. D. Spreading-rate dependence of melt extraction at mid-ocean ridges from mantle seismic refraction data. *Nature* **432,** 744–747 (2004).
51. Yu, C. *et al.* Deep thermal structure of Southeast Asia constrained by S-velocity data. *Mar. Geophys. Res.* **38,** 341–355 (2017).
52. Sotin, C. & Parmentier, E. M. Dynamical consequences of compositional and thermal

density stratification beneath spreading centers. *Geophys. Res. Lett.* **16,** 835–838 (1989).

53. McKenzie, D. P. The generation and compaction of partial melts. *J. Petrol.* **25,** 713–765 (1984).

54. Ohuchi, T. *et al.* Dislocation-accommodated grain boundary sliding as the major deformation mechanism of olivine in the Earth's upper mantle. *Sci. Adv.* **1,** e1500360–e1500360 (2015).

55. Huismans, R. & Beaumont, C. Depth-dependent extension, two-stage breakup and cratonic underplating at rifted margins. *Nature* **473,** 74–8 (2011).

56. Nissen, S. S. *et al.* Gravity, heat flow, and seismic constraints on the processes of crustal extension: Northern margin of the South China Sea. *J. Geophys. Res.* **100,** 22447 (1995).

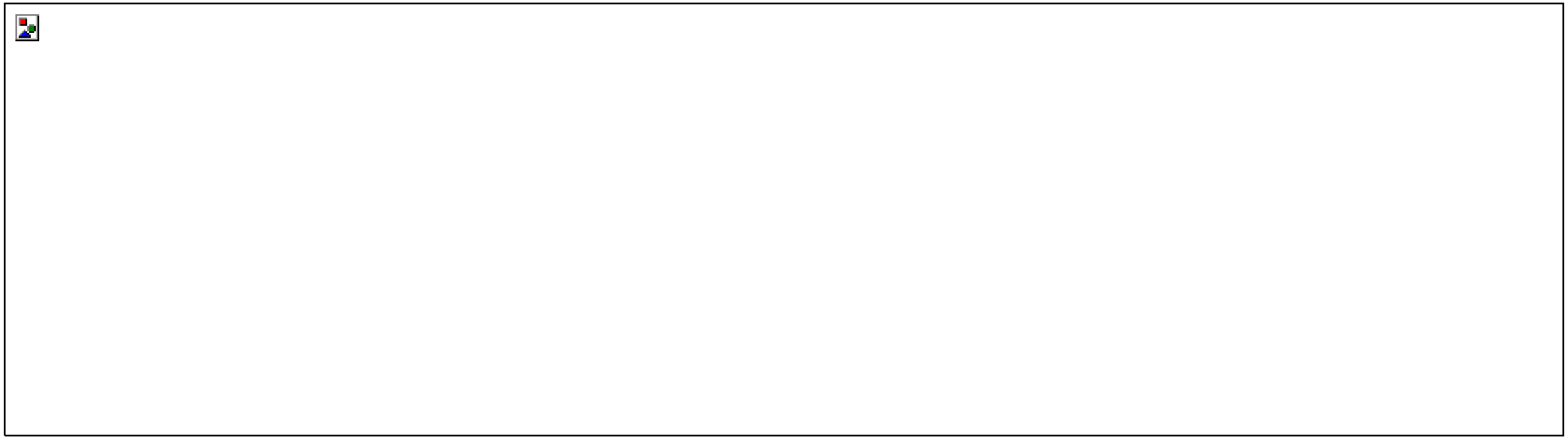

Supplementary material 1: Un-interpreted regional seismic reflection profile crossing the northern SCS margin with the location of IODP Sites[17] and magnetic chrons[19]

Supplementary material 2: A, B and C un-interpreted seismic profiles crossing Ridges A,B and C showing the continuity of these structures along the northern SCS margin. D, un-interpreted seismic line located on the OMH, arrows indicated tilted and folded reflectors truncated by Tg. Map of time depth to acoustic basement (Tg) showing seismic lines, Sites and magnetic chron locations.

Table1-01

Supplementary material 3: Table of bulk-rock major and trace element compositions of magmatic rocks from IODP expeditions 367/368, Sites U1500 and U1502. (ppm=µg/g, detailed method provided in the method section of the proceedings of Expeditions 367/368[17])

Author contributions

HCL.: Co-PI of the original drilling proposal, interpretation of seismic data, co-chief scientist of Exp 367/368, directed the writing of the paper

GM: Principal co-author, developed geodynamic model jointly with HCL and MN. Shipboard scientist (structural geology) at Exp. 368

MN: Shipboard scientist (structure/sedimentology) at Exp. 367. Structural interpretation of syn-rift sedimentation, contributed to model development and graphics

ZS: Co-PI of the original drilling proposal, interpretation of seismic data, co-chief scientist of Exp 367/368

JS: Co-chief scientist of Exp 367/368; co-proponent of original drilling proposal

ZJ: Co-chief scientist of Exp 367/368, coordinated biostratigraphic interpretations

AK: Expedition 367/368 project manager

CAZ: Expedition 367/368 project manager and biostratigraphy

J.B., A.B., Y.C., M.D., A.F., J.H., T.W.H., K.H., B.H., X.H., B.J., Ch. Lei., L.L., Z.L., A.L., Cl.L., A.McC., M.N., C.R., I.S., St.S., C.S., X.S., R.X., R.Y., L.Y., C.Z., J.Z., Y.Z., N.Z., and L.Z. collected the drilling data during IODP Exp. 367 and participated to the writing of the paper. S.B., D.C., K.D., W.D., E.F., F.F., A.J., E.H., S.J., H.J., R.K., B.L., Y.L., J.L (co-PI)., Chang Liu, Chuanlian Liu, L.N., N.O., D.W.P., P.P., N.Q., Sa.S., J.C.S., Su.S., L.T., F.M.vdZ., S.W., H.W., and G.Z. collected the drilling data during IODP Exp. 368 and participated to the writing of the paper. Roles on board are detailed in https://iodp.tamu.edu/scienceops/precruise/southchinasea2/participants.html.

Expedition 367/368 Scientists Addresses

c CAS Key Laboratory of Ocean and Marginal Sea Geology, South China Sea Institute of Oceanology, China
d Division of Geological and Planetary Sciences, California Institute of Technology, USA
e School of Ocean and Earth Science, Tongji University, 1239 Siping Road, Shanghai 200092, China
f International Ocean Discovery Program, Texas A&M University, 1000 Discovery Drive, College Station TX 77845, USA
g Dipartimento di Geologia Paleontologia e Geofisica, Università degli Studi di Padova, Italy,
h School of Geosciences, University of Aberdeen, Aberdeen, Scotland, United Kingdom, AB24 3UE.
i Observatoire Midi-Pyrenees, CNRS, France

j Guangzhou Institute of Geochemistry, Chinese Academy of Sciences, P.R. China
k Petroleum & Marine Research Division, Korea Institute of Geoscience and Mineral Resources (KIGAM), 124 Gwahak-ro, Yuseong-gu, Daejeon 34132, Republic of Korea
l School of Geosciences, University of Sydney, NSW 2006, Australia
m Key Laboratory of Submarine Geoscience, Second Institute of Oceanography (SIO), State Oceanic Administration (SOA), Baochubei Road 36, Hangzhou, China
n Department of Geology, Brigham Young University, USA
o Department of Geology, Southern Illinois University at Carbondale, 1259 Lincoln Drive, Parkinson Lab, Carbondale IL 62901, USA
p Institute for Geosciences, Universidade Federal Fluminense (UFF), Brazil, CAPES Foundation, Ministry of Education of Brazil, Brasilia - DF, Zip Code 70.040-020
q Department of Geoscience, Shimane University
r Earth and Atmospheric Sciences, University of Nebraska, Lincoln, 214 Bessey Hall, Lincoln NE 68588, USA
s JAMSTEC, Yokohama, Kanagawa 236-0001 Japan
t Department of Geology, Peking University, P.R China
u Guangzhou Institute of Geochemistry, Chinese Academy of Sciences, P.R China
v Institute of Groundwater and Earth Sciences, Jinan University, 601 West Huangpu Dadao, Guangzhou GD 510632, China
w Geology and Geography, West Virginia University, USA
x GEOMAR Helmholtz Center for Ocean Research Kiel, Christian-Albrechts-Universität zu Kiel, Wischhofstrasse 1-3, Kiel 24148, Germany
y Department of Marine Science and Engineering, China University of Geosciences, P.R. China
z Department of Micropalaeontology Nanjing Institute of Geology and Palaeontology, Nanjing, P.R. China
aa School of Geographical and Oceanographical Sciences, Nanjing University, China
ab Department of Geology and Geophysics, Woods Hole Oceanographic Institution, 360 Woods Hole Road, Woods Hole MA 02543, USA
ac Department of Geology and Geophysics, Louisiana State University, E235 Howe-Russell-Kniffen, Geoscience complex, Baton Rouge LA 70803
ad Department of Geology, University of South Florida, Tampa, USA
ae Department of Earth and Environmental Sciences, Università degli studi di Pavia, Italy
af Institute of Earth Sciences, University of Lausanne, Switzerland
ag Department of Marine Geophysics, National Centre for Antarctic and Ocean Research (NCAOR), Vasco Da Gama GOA 403804, India
ah Petrophysics(Physical Properties) Specialist, Faculty of Science, Graduate School of Science and Technology for Innovation, 1677-1 Yoshida, Yamaguchi-shi,Yamaguchi 753-8512, Japan
ai Earth & Environmental Sciences, University of Iowa, 115 Trowbridge Hall, Iowa City IA 52242, USA
aj School of Earth Sciences Ohio State Universit, USA
ak Department of Engineering and Geology, University of Chieti-Pescara, Via dei Vestini 31, Chieti Scalo 66013, Italy
al Institute of Marine and Antarctic Studies (IMAS), University of Tasmania, Australia
am Department of Geology, California State University, Sacramento, USA

an Lamont-Doherty Earth Observatory, Columbia University, 61 Route 9W, Palisades NY 10964, USA
ao Institute of Oceanography National Taiwan University, Tapei, Taiwan
ap Institute of Deep-sea Science and Engineering, Chinese Academy of Sciences, China
aq Institute of Geosciences, Christian Albrechts University Kiel, Ludwig-Meyn-Strasse 10, Kiel 24118, Germany
ar Institute of Oceanology, Chinese Academy of Sciences, 7 Nanhai Road, Qingdao Shandong Province 266071, China
as School of Ocean Sciences, China University of Geosciences, 29 Xueyuan Road, Haidian District, Beijing, China
at Department of Earth and Atmospheric Sciences, Purdue University, USA
au Institute of Oceanology Chinese Academy of Sciences, Guangzhou, P.R. China